

In situ rheological measurements at extreme pressure and temperature using synchrotron X-ray diffraction and radiography

Paul Raterron* and Sébastien Merkel

Laboratoire de Structure et Propriétés de l'Etat Solide, CNRS 8008, Université de Lille 1, F-59655 Villeneuve d'Ascq Cedex, France. E-mail: paul.raterron@univ-lille1.fr

Dramatic technical progress seen over the past decade now allows the plastic properties of materials to be investigated under extreme pressure and temperature conditions. Coupling of high-pressure apparatuses with synchrotron radiation significantly improves the quantification of differential stress and specimen textures from X-ray diffraction data, as well as specimen strains and strain rates by radiography. This contribution briefly reviews the recent developments in the field and describes state-of-the-art extreme-pressure deformation devices and analytical techniques available today. The focus here is on apparatuses promoting deformation at pressures largely in excess of 3 GPa, namely the diamond anvil cell, the deformation-DIA apparatus and the rotational Drickamer apparatus, as well as on the methods used to carry out controlled deformation experiments while quantifying X-ray data in terms of materials rheological parameters. It is shown that these new techniques open the new field of *in situ* investigation of materials rheology at extreme conditions, which already finds multiple fundamental applications in the understanding of the dynamics of Earth-like planet interior.

© 2009 International Union of Crystallography
Printed in Singapore – all rights reserved

Keywords: materials; plastic deformation; high pressure; high temperature; rheology; synchrotron X-ray; diffraction; imaging; stress; strain; strain rate.

1. Introduction

Recent technical advances in high-pressure devices coupled with synchrotron radiation allow investigation of materials rheology at pressure (P) and temperature (T) in excess of 135 GPa and 1870 K, respectively. Specimens of a few cubic millimeters in multi-anvil apparatuses, or of thousands of cubic micrometers in the diamond-anvil cell, can now be deformed at pressures corresponding to those existing hundreds or thousands of kilometers within Earth-like planets. During deformation, the applied differential stress (t) and resulting specimen strain (ε) and strain rate ($\dot{\varepsilon}$) are quantified *in situ* by time-resolved X-ray diffraction and radiography. Although the basic principles of these measurements are straightforward, *i.e.* t is deduced from diffraction peak shifts arising from polycrystalline materials within the cell, and ε is measured optically on a fluorescent YAG crystal placed downstream with respect to the specimen, carrying out these measurements at extreme conditions has been challenging. This has required adapting the high-pressure devices to allow deformation of specimens and collection of the diffracted beams in specific orientations with respect to the principal stress directions, as well as developing the tools to quantify the

stress tensor from small d -spacing variations between different populations of grains within deforming aggregates.

These new techniques renewed interest in research involving the *in situ* investigation of materials rheological properties at extreme conditions. They have multiple potential applications in Earth sciences when investigating the dynamics of planet interiors, as well as in materials science for the search for new super-hard materials or for quantifying armor resistance during shell explosions. Here we review the state-of-the-art of the high-pressure devices available today for these types of measurements, the techniques involved, and their resolutions to quantify stress, texture, specimen strain and strain rate, whether using a monochromatic or a white X-ray beam to collect the data.

2. Extreme-pressure deformation devices

We focus here on apparatuses which allow deforming materials at pressure largely in excess of 3 GPa. Until recent years, controlled deformation experiments in Paterson-type gas medium apparatuses or Griggs-type solid medium apparatuses (*e.g.* Bistricky *et al.*, 2000; Jung & Green, 2009) were limited to typically 3 GPa pressure. Previous attempts to use the

alternatively forward and backward (e.g. Li *et al.*, 2006a) is also possible in the D-DIA, which allows for instance investigating materials strain hardening. One of the remarkable features of the D-DIA is its ability to promote constant specimen strain rate usually corresponding at high temperature to constant applied stress (within uncertainties), *i.e.* steady-state deformation conditions, which is critical when investigating materials deformation laws. The typical P and T ranges accessible in the D-DIA at control conditions are, respectively, 2 to 19 GPa and room- T to 1873 K, for steady-state strain rates typically in the range 10^{-6} to 10^{-4} s $^{-1}$. For on-line experiments, the back lateral anvils of the D-DIA must be transparent to the X-ray beam, *i.e.* made of sintered diamond or cubic boron nitride (cBN), in order to allow lateral diffraction (see §3).

2.3. Rotational Drickamer apparatus

The Drickamer apparatus consists of two opposed anvils contained in a cylindrical sleeve. The anvil ends facing each other are cut at a low angle (20°) to form a conical surface which is supported by gasket material, while the flat tips of the anvils define the top and bottom surface of the confined medium. This apparatus can reach pressures and temperatures of 30 GPa and 1700 K, respectively (Gotou *et al.*, 2006). It has been used for axial deformation of samples under high pressure and measurements with polychromatic beam (Funamori *et al.*, 1994; Uchida *et al.*, 1996), and recently adapted for monochromatic beam and X-ray radiography (Nishiyama *et al.*, 2009). It was also modified (Yamazaki & Karato, 2001; Xu *et al.*, 2005) in order to accommodate shear deformation of the confined medium, and became the rotational Drickamer apparatus (RDA, Fig. 2). Shearing of the confined material is promoted by rotating the bottom anvil (connected to a servomotor and a gear box) relative to the top anvil.

Such geometry allows near simple shear deformation of disc-shaped samples less than 1 mm thick and ~ 4 mm in diameter. In the RDA, samples also undergo some uniaxial compression and its component increases with the sample thickness. In order to avoid the radial pressure gradient present within disc-shaped samples, and to promote homogeneous deformation of the specimen, ring-shape samples are usually used in the RDA. The remarkable feature of the RDA is its ability to allow specimen large strain deformation (exceeding $\gamma \simeq 6$). The typical P and T accessible in the RDA are, respectively, 16 GPa and 1873 K, for steady-state equivalent strain rates of the order of 5×10^{-5} s $^{-1}$ (e.g. Nishihara *et al.*, 2008).

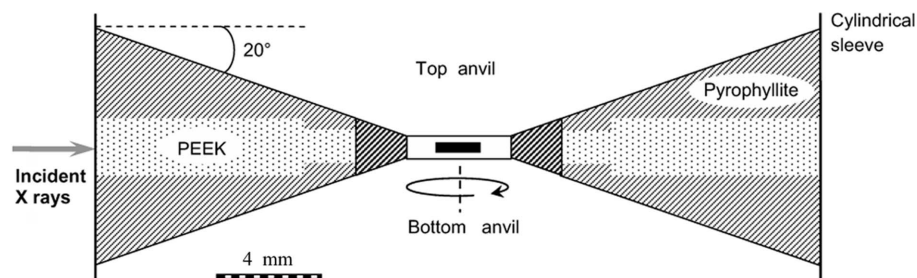


Figure 2

Schematic cross section of a typical cell assembly in the rotational Drickamer apparatus (RDA, after Nishihara *et al.*, 2008). Dimensions are approximate. The outer cylindrical sleeve, made of a hard Al-alloy almost transparent to high-energy X rays, is not represented. Gasket materials consist of polyether ether ketone (PEEK), which has low X-ray absorption, and pyrophyllite (dark hatched when fired). The white rectangle in between top and bottom anvils shows the disc-shape pressure medium (~ 1 mm thick), while the black rectangle at its center represents a disc-shape sample. In the RDA, rotation of the bottom anvil with respect to the top anvil promotes shear deformation of the sample. See text for more explanations and for details: Yamazaki & Karato (2001), Xu *et al.* (2005) and Nishihara *et al.* (2008).

3. Stress, texture and strain measurements

3.1. Stress measurement with a monochromatic beam

In diffraction, polycrystalline samples subjected to stress show distortions of Debye rings. For instance, Fig. 3 presents the unrolled diffraction image obtained for a sample of h.c.p.-Co at 42.6 GPa in the DAC (Merkel *et al.*, 2006b). Stress appears as sinusoidal variations in d -spacings that are smaller (and correspondingly diffraction angles θ are larger) perpendicular to the compression direction (dark arrows). The changes in d -spacings depend upon the applied compressive stress, elastic properties and the plastic deformation of the sample. Plastic deformation is also expressed in intensity variations that signify preferred orientation, attained, for example, through dislocation glide, and can be fully interpreted based on microscopic deformation mechanisms (Wenk *et al.*, 2006).

Interpretation of the sinusoidal variations in d -spacings (lattice strains) has been a matter of debate. Elastic theories have been developed to relate the measured lattice strains to stress and elastic properties (Singh *et al.*, 1998). In axial geometry, the stress applied to the sample can be expressed as

$$\sigma = \begin{bmatrix} P & 0 & 0 \\ 0 & P & 0 \\ 0 & 0 & P \end{bmatrix} + \begin{bmatrix} -t/3 & 0 & 0 \\ 0 & -t/3 & 0 \\ 0 & 0 & 2t/3 \end{bmatrix}, \quad (1)$$

where P is the hydrostatic pressure and $t = \sigma_{33} - \sigma_{11}$ is the differential stress. For a polycrystal, a diffraction line is the sum of the contribution of all crystallites in the condition of diffraction: crystallites whose normal to the diffracting plane (hkl) is parallel to the scattering vector. Their d -spacings depend on the local environment and their elastic properties. The measured value is then the arithmetic average of all those individual d -spacings.

In the elastic model, one can show that, for a polycrystal free of lattice preferred orientations, the measured d -spacings can be expressed as

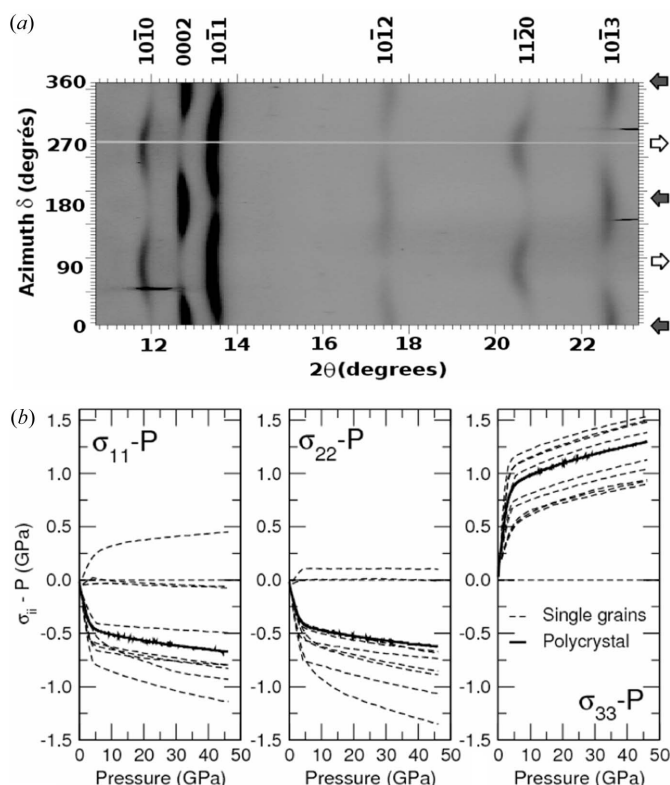


Figure 3
 (a) Example of an unrolled radial diffraction image for a sample of h.c.p.-Co at 42.6 GPa in the diamond anvil cell. The image shows the diffraction as a function of the Bragg angle 2θ and the azimuth angle on the image plate δ (Fig. 2). The sinusoidal variations in positions of the diffraction lines are due to elastic deformation and stress in the sample; intensity differences along lines indicate preferred orientation caused by plastic deformation. The compression direction is indicated by the dark arrows.
 (b) Average stress (thick solid lines) and local stress components in single grains (thin dashed lines) versus pressure for a Co polycrystal plastically deformed in the diamond anvil cell. Results of EPSC calculations optimized to lattice strains measured experimentally (Merkel *et al.*, 2009).

$$d_m(hkl, \psi) = d_p(hkl)[1 + Q(hkl)(1 - 3 \cos^2 \psi)], \quad (2)$$

where d_m is the measured d -spacing of the hkl line, d_p is the d -spacing of the hkl line under hydrostatic pressure P , ψ is the angle between the diffracting plane normal and the maximum stress direction, and $Q(hkl)$ is the lattice strain parameter. $Q(hkl)$ is a measure of the amplitude of the sinusoidal variations in d -spacings for the hkl diffraction line (Fig. 3) and, in this model, is a function of the single-crystal elastic moduli and the differential stress t . For materials with known elastic properties, the lattice strain parameters $Q(hkl)$ fitted to the measured d -spacings can be used to evaluate the differential stress t using the mathematic expressions of Singh *et al.* (1998).

Elastic theories that include effects of lattice preferred orientations have also been developed (Matthies *et al.*, 2001). In this case, the measured d -spacings are not linear with $(1 - 3 \cos^2 \psi)$, but one can still find a relation between the differential stress, measured d -spacings and single-crystal elastic moduli. It should be noted, however, that, in the elastic theory, effects of lattice preferred orientations on the measured lattice

strains are small and can be difficult to distinguish experimentally.

However, elastic theories are based on lower or upper bound assumptions and have shown severe limitations. In particular, it was shown that stresses deduced from diffraction images on h.c.p.-Co (Fig. 3a) were inconsistent, ranging from 1.7 to 4.3 GPa depending on the diffraction line used for the analysis (Merkel *et al.*, 2006b). This issue was also previously observed on MgO (Weidner *et al.*, 2004) and was recently solved by introducing elastoplastic self-consistent (EPSC) models for the analysis (Li *et al.*, 2004a; Burnley & Zhang, 2008; Merkel *et al.*, 2009). EPSC models represent the aggregate by a discrete number of orientations with associated volume fractions. The latter are chosen such as to reproduce the initial texture of the aggregate. EPSC treats each grain as an ellipsoidal elastoplastic inclusion embedded within a homogeneous elastoplastic effective medium with anisotropic properties characteristic of the textured aggregate. The external boundary conditions of stress and strain are fulfilled on average by the elastic and plastic deformations at the grain level. The self-consistent approach explicitly captures the fact that soft-oriented grains tend to yield at lower stresses and transfer load to plastically hard-oriented grains, which remain elastic up to rather large stress. The model uses known values of single-crystal elastic moduli and parameters associated with each active plastic deformation. The simulated internal strains are compared with experimental data by identifying the grain orientations which, in the model aggregate, contribute to the experimental signal associated with each diffracting vector. Parameters controlling the nature of the plastic behavior of the polycrystal (choice of deformation mechanisms, their strength, and hardening parameters) are optimized to reproduce the measured d -spacings in the calculation.

For instance, Fig. 3(b) presents the average stress versus pressure in a Co polycrystal plastically deformed in the DAC obtained by adjusting EPSC calculations to experimental lattice strain measurements (Merkel *et al.*, 2009). The average differential stress and $t = \sigma_{33} - \sigma_{11}$ is well constrained. Fig. 3(b) also presents the local stress for eight randomly selected orientations in the polycrystal. Although the average stress in the polycrystal follows the symmetry expected for DAC experiments ($\sigma_{11} = \sigma_{22}$ and $\sigma_{33} > \sigma_{11}$), stresses in individual grains do not agree with this geometry and show considerable heterogeneities. Elastic models completely overlook this phenomenon and, therefore, should be avoided for data interpretation.

EPSC models treat each orientation as an ellipsoidal elastoplastic inclusion embedded within a homogeneous elastoplastic effective medium. As such, local interactions from grain to grain and heterogeneities within the grains themselves are not accounted for. Three-dimensional full-field polycrystalline models can predict local-field variations (*e.g.* Castelnau *et al.*, 2008). These calculations show important heterogeneities within grains and a strong localization of stress and strain near the grain boundaries. However, the precision of those models comes with large computational cost and complexity, and they cannot be systematically applied for

interpreting experimental results. Moreover, input parameters are not always known for high-pressure materials. Self-consistent models such as EPSC could also be improved to account for grain rotations and viscous relaxation, which could influence the interpretation of high-pressure experiments. Those are under development and should be available in the near future.

3.2. Stress measurement with a white beam

The principle of this measurement is identical to that described in the previous section. The differential stress t is deduced from d -spacing variations among different populations of grains of a given aggregate (often the specimen), which translates into shifting of X-ray diffraction peaks, measured here using energy-dispersive X-ray (EDX) spectrometry. This requires using a conical back slit which imposes the diffraction angle (e.g. $2\theta \simeq 6^\circ$), and behind the conical slit a multi-detector (Fig. 4). The position of a given EDX detector along a section of the diffraction cone defines the azimuthal angle δ of the corresponding spectrum (see Fig. 2), which is related to the angle ψ between the diffracting plane normal and the maximum stress direction. Hence, using equation (2), the lattice strain parameters $Q(hkl)$ fitted to the measured d -spacings can be used to evaluate the differential stress t in materials with known elastic properties (e.g. Funamori *et al.*, 1994; Uchida *et al.*, 1996; Chen *et al.*, 2004; Li *et al.*, 2004b; Weidner *et al.*, 2005; Burnley & Zhang, 2008).

In reality, the number of EDX detectors along the diffraction cone is limited (Fig. 4), which limits the accuracy on the determination of t in the case of complex stress field, e.g. with unknown principal directions and/or with radial stress gradient within the aggregate. Using a white beam is, however, well adapted for determining stress in simple geometry experiments (e.g. uniaxial compression in the D-DIA). The conical slit also defines the diffracting volume as the inter-

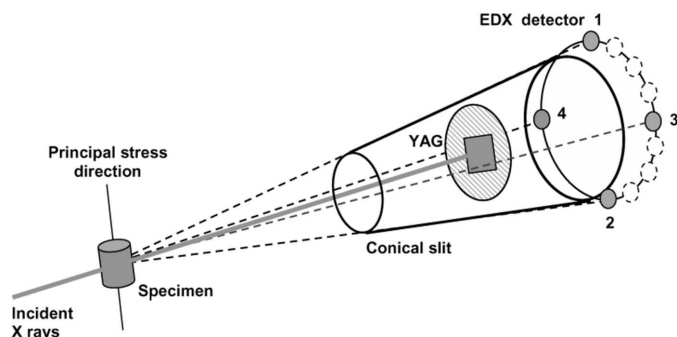


Figure 4

Experimental set-up for measuring the differential stress using a white X-ray beam. Diffraction at fixed angle ($2\theta \simeq 6^\circ$) is obtained using a conical slit with the specimen placed at the tip of the cone. Energy-dispersive spectra are recorded using a multi-detector placed behind the conical slit. Approximate detector positions which define the azimuthal angles δ (see Fig. 1) are indicated by small circles (not to scale). During uniaxial compression, a measure of the differential stress t can be obtained using only two detectors (e.g. detectors 1 and 3, or 1 and 4), although four detectors (1 to 4) are often used. Specimen images are collected on the fluorescent YAG, magnified and recorded using a CCD camera.

section between the diffraction cone and the incident X-ray beam. Therefore, when the specimen is properly centered at the tip of the cone, this allows filtering of unwanted contributions to the EDX spectra, as for instance that of the confining medium. This characteristic is particularly useful for experiments in a large-volume press (D-DIA and RDA), where the specimen is often buried under layers of diffracting materials which constitute the confining medium.

Using this technique, for each set of diffraction spectra (one spectrum per EDX detector) one can deduce the hydrostatic pressure P , calculated from the average volume of the material unit cell at run T using the corresponding equation of state, and a set of stress values (using the material known elastic constants) arising from the measured d -spacing of the observable hkl peaks (Fig. 5). Part of the discrepancy on stress values within each set arises from the accuracy on d -spacing measurement, which depends on both diffraction-angle and spectrum-energy resolutions. Yet, a significant part of stress

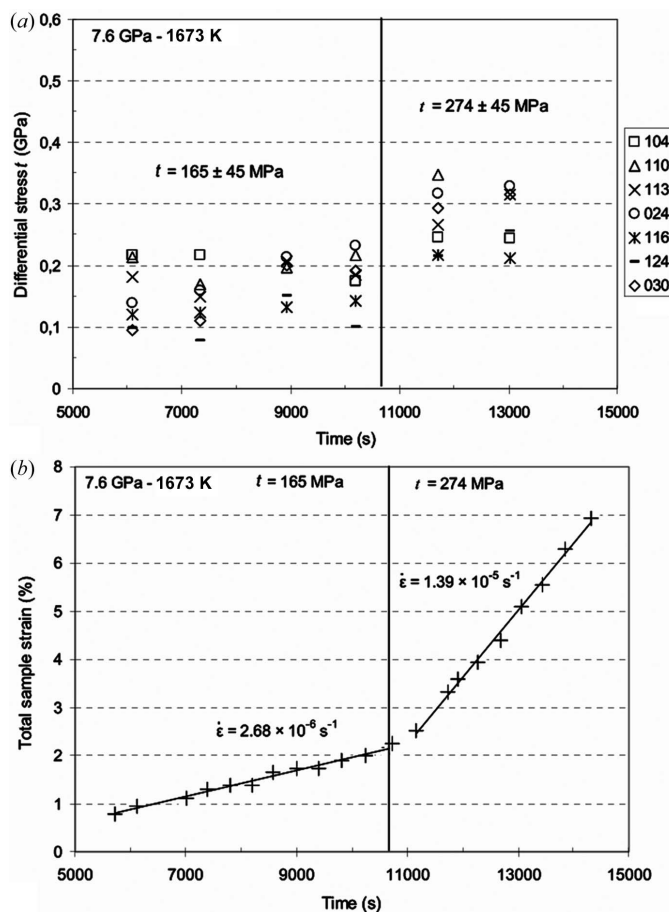


Figure 5

(a) Differential stress *versus* time as measured with a white X-ray beam within the alumina pistons compressing a forsterite sample in the D-DIA at the indicated P and T conditions. Exploitable alumina hkl peaks are indicated. Discrepancy in stress measurements at a given time results from both accuracy on the measurement and the properties of the stressed alumina polycrystal. Average differential stress t values are indicated for each steady-state regime of deformation. (b) Corresponding strain *versus* time plots as measured by X-ray radiography (§3.4) of the forsterite sample. Steady-state deformation translates here by constant strain rates (indicated slopes).

discrepancy arises from stress heterogeneity between different populations of grains within the aggregate, as explained above (§3.1). If enough *hkl* peaks are exploitable (typically more than ten peaks), it is assumed that a reasonable value for the differential stress t is obtained by averaging the stress values of a given data set; EPSC modeling (see above) is a more accurate way of deducing the actual differential stress (Burnley & Zhang, 2008) and should be used more routinely in the future. As of today, the reported uncertainties on t values measured at high P by X-ray diffraction are still large, *i.e.* typically ± 50 MPa for low applied stress (*e.g.* Fig. 5) and as high as hundreds of MPa for high stress levels.

3.3. Lattice preferred orientation and texture

Lattice preferred orientation (LPO) can be quantified with the intensity variations along the Debye rings. Information can be extracted from either monochromatic or white beam measurements if enough orientations have been measured (*i.e.* with enough azimuthal angles δ), although monochromatic data are in practice more adapted for quantifying LPO. Typically, it is assumed that measurements every 5 or 10° in ψ are sufficient for the analysis.

LPO arises from the plastic deformation of the sample. The observed LPO can be compared with polycrystal plasticity simulations to obtain information about slip systems operating in the sample. This is particularly relevant for mineral physics since seismic anisotropy in the deep Earth arises from the LPO of minerals owing to the convection flow. The first *in situ* LPO measurements at high pressure using synchrotron radiation were performed on the h.c.p. phase of Fe (Wenk *et al.*, 2000). Since then, the technique has been applied numerous times, both on metals and minerals [see Wenk *et al.*, (2006) for a review].

The LPO can be represented by an orientation distribution function (ODF). The ODF is required to estimate anisotropic physical properties of polycrystals such as elasticity or plasticity (Kocks *et al.*, 1998). The ODF represents the probability of finding a crystal orientation, and it is normalized such that an aggregate with a random orientation distribution has a probability of 1 for all orientations. If LPOs are present, some orientations have probabilities higher than 1 and others lower than 1. The ODF can be calculated using the variation in diffraction intensity with orientation using tomographic algorithms such as *WIMV* (Matthies & Vinel, 1982) as implemented in the *BEARTEX* package (Wenk *et al.*, 1998) or in the *Maud* Rietveld refinement program (Lutterotti *et al.*, 1999). This technique has been successfully applied to measure textures and deduce active high-pressure deformation mechanisms (Wenk *et al.*, 2006).

3.4. Strain measurements

For large-volume apparatuses (*e.g.* D-DIA and RDA), specimen plastic strain is measured *in situ* on time-resolved X-ray radiographs (absorption contrast imaging) collected on a fluorescent YAG crystal placed downstream with respect to the cell assembly (*e.g.* Vaughan *et al.*, 2000; Raterron *et al.*,

2007). For this measurement the X-ray front slits are removed, which in the RDA results in exposing the whole section of the cell assembly to the beam. In the D-DIA, the sample is usually only visible through the gap in between the front lateral anvils (Fig. 6), classically made of tungsten carbide (WC); for on-line D-DIA, X-ray-transparent lateral anvils (sintered diamond or cBN) are thus preferred. With dense specimens promoting enough contrast, images can be directly observable on the YAG crystal and ultimately recorded on a CCD camera after magnification. In case of insufficient contrast, strain markers (*e.g.* thin X-ray absorbent metal foils which appear as dark lines on the radiographs) are placed within the cell in order to visualize sample strain during deformation. In the D-DIA, strain markers are placed horizontally at sample ends (Fig. 6), while in the RDA one vertical strain marker is placed within the disc- or ring-shaped sample (*e.g.* Nishihara *et al.*, 2008).

For a large enough strain, specimen images are treated with commercial software to measure strain and strain rate. This operation can be performed live, *i.e.* during the experiment. In the D-DIA, sample strain $\varepsilon(t)$ can be deduced from sample length $l(t)$ using the well known relationship: $\varepsilon(t) = \ln l_0/l(t)$ [here in compression $\varepsilon(t) \geq 0$], where l_0 is the initial length of the specimen at given conditions. Strain rates ($\dot{\varepsilon}$) and their uncertainties are then deduced from $\varepsilon(t)$ versus time plots (Fig. 5b). Given the resolution of the image (one pixel corresponds to a few micrometers), the size of the specimen and the usual strain rate condition, and taking into account the limited amount of beam time for each experimental point (a few hours), uncertainty is about 10^{-6} s^{-1} or better on the strain rate. In the RDA, sample equivalent strain is deduced from the rotation of the vertical strain marker during defor-

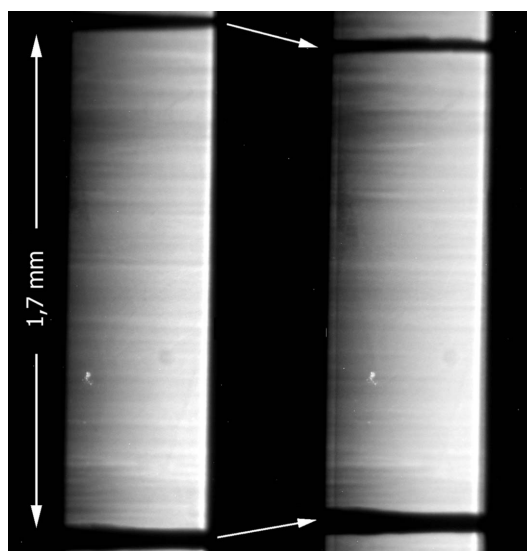


Figure 6

Two radiographs of an Mg_2SiO_4 forsterite sample taken at different times during deformation at 7 GPa pressure and 1673 K, as obtained through the gap in between the lateral anvils of the D-DIA that equips beamline X17-B2 of the NSLS (Upton, NY, USA). The black horizontal lines are the image of thin Re foils placed at sample ends and used as strain markers. White arrows indicate the sample shortening ($\sim 10\%$ strain). Note the anvil gap opening during deformation while lateral anvils are moving backwards.

mation. This rotation is a function of both specimen shear strain and uniaxial compression (details in Nishihara *et al.*, 2008). Conversion of the marker rotation to specimen equivalent strain and strain rate is not straightforward. Consequently, the uncertainty on the absolute equivalent strain rate can be fairly large in the RDA, *i.e.* about 40% of the strain rate.

In the DAC, samples are less than 30 μm thick and typically too small for recording X-ray radiograph images. In this case, samples dimensions are estimated by moving the DAC in front of the incident X-ray beam and analyzing the transmitted intensity. High-density samples such as Co or Fe have a high contrast compared with their environment (diamonds and gaskets) and their dimensions can be measured (*e.g.* Merkel & Yagi, 2005). Low-density samples cannot be distinguished from their environment. In this case, sample strain cannot be evaluated. Besides, steady-state strain rate conditions at constant P are not achievable in the DAC since increasing strain also results in increasing P . In the DAC, the imaging system is, thus, mostly used to evaluate the sample strain during deformation (and not to quantify the strain rate).

4. Applications and concluding remarks

These recent technical developments in on-line high-pressure deformation apparatus have been largely driven by the Earth sciences community, with the aim to better understand the dynamics of planet interiors where extreme conditions of P and T are prevailing. Consequently, a large majority of the studies published so far find applications in the mineral physics field. Drickamer presses under uniaxial loading have been used to study the mechanical properties of NaCl (Funamori *et al.*, 1994), MgO and Mg_2SiO_4 (Uchida *et al.*, 1996). The DAC in a radial diffraction geometry has been used to investigate the plastic properties of common metals such as iron and tungsten (Hemley *et al.*, 1997), gold, rhenium and molybdenum (Duffy *et al.*, 1999*a,b*), platinum (Kavner & Duffy, 2003), copper (Speziale *et al.*, 2006*a*), h.c.p.-cobalt (Merkel *et al.*, 2006*b*) or osmium (Weinberger *et al.*, 2008), core and mantle phases such as h.c.p.-Fe (Wenk *et al.*, 2000; Merkel *et al.*, 2004; Miyagi, Kunz *et al.*, 2008), olivine (Wenk *et al.*, 2004), hydrous and anhydrous ringwoodite (Kavner & Duffy, 2001; Kavner, 2003; Wenk *et al.*, 2004), stishovite (Shieh *et al.*, 2002), MgO (Merkel *et al.*, 2002), silicate perovskite (Merkel *et al.*, 2003; Wenk *et al.*, 2004), calcium silicate perovskite (Shieh *et al.*, 2004; Miyagi *et al.*, 2009), magnesio-wustite (Tommaso *et al.*, 2006), calcium oxide (Speziale *et al.*, 2006*b*), garnet (Kavner, 2007) and silicate post-perovskite (Merkel *et al.*, 2007), as well as other materials such as boron suboxide (He *et al.*, 2004), cubic silicon nitride (Kiefer *et al.*, 2005), argon (Mao *et al.*, 2006), MgGeO_3 post-perovskite (Merkel *et al.*, 2006*a*) or calcium fluorite (Kavner, 2008). The D-DIA has been used to investigate the plasticity of Earth mantle minerals such as olivine and its high-pressure polymorph ringwoodite (Wenk *et al.*, 2005; Li *et al.*, 2006*b*; Nishiyama *et al.*, 2005; Raterron *et al.*, 2007, 2009; Durham *et al.*, 2009), pyrope garnet and diopside (Li *et al.*, 2006*a*; Amiguet

et al., 2009), serpentine (Hilairt *et al.*, 2007) which forms in subduction zones by oceanic lithosphere alteration, the CaIrO_3 analogue of silicate post-perovskite (Miyagi, Nishiyama *et al.*, 2008; Walte *et al.*, 2009), as well as MgO, quartz and iron (Uchida *et al.*, 2004; Nishiyama *et al.*, 2007; Burnley & Zhang, 2008; Mei *et al.*, 2008), three materials which have long received attention in both earth sciences and materials science. The D-DIA has also been used to quantify energy dissipation induced by high-pressure phase transformation in materials, and its implication for seismic wave dissipation in the Earth's mantle (Li & Weidner, 2007, 2008). The RDA, to our knowledge, has so far been used to investigate the plastic properties of olivine and its high-pressure polymorph wadsleyite (Nishihara *et al.*, 2008; Kawazoe *et al.*, 2009).

Recent efforts have been devoted to improving the accuracy and relevance of the measurement: external heating in the DAC (Liermann *et al.*, 2009), specific conical slits and multi-detector to improve the diffraction angle resolution for the D-DIA and the RDA at the NSLS and the APS, and numerical modeling of stress and strain in polycrystalline samples (Burnley & Zhang, 2008; Merkel *et al.*, 2009). In the near future, a new D-DIA system will be available at the ESRF, while new apparatuses are being developed such as the future deformation-TCup, a Kawai-type multi-anvil press with deformation capability up to 20 GPa pressure (see Wang *et al.*, 2007). These improvements will allow exciting new experiments, and a better understanding of the effect of pressure on materials plastic properties, with likely more fundamental implications in both deep earth minerals physics and material sciences.

We gratefully acknowledge the Consortium for Material Properties Research in Earth Sciences (COMPRES, <http://www.compres.stonybrook.edu/>), two anonymous reviewers for their thorough reviews of the manuscript and suggestions to improve it, as well as the scientists in charge of X-ray synchrotron beamlines dedicated to high-pressure studies for providing the community with remarkable tools to investigate materials rheological properties at extreme P and T conditions. This work was supported by the French ANR Grants 'Jeunes Chercheurs DiUP' and 'Mantle Rheology' (No. BLAN08-2_343541), and the CNRS 'Programme International de Collaboration Scientifique' (PICS project).

References

- Amiguet, E., Raterron, P., Cordier, P., Couvy, H. & Chen, J. (2009). *Phys. Earth Planet. Inter.* doi:10.1016/j.pepi.2009.08.010.
- Bistricky, M., Kunze, K., Burlini, L. & Burg, J. P. (2000). *Science*, **290**, 1564–1567.
- Burnley, P. C. & Zhang, D. (2008). *J. Phys. Condens. Matter*, **20**, 285201.
- Bussod, G. Y., Katsura, T. & Rubie, D. C. (1993). *Pure Appl. Geophys.* **41**, 579–599.
- Castelnau, O., Blackman, D. K., Lebensohn, R. A. & Ponte Castañeda, P. (2008). *J. Geophys. Res.* **113**, B09202.
- Chen, J., Li, L., Weidner, D. & Vaughan, M. (2004). *Phys. Earth Planet. Inter.* **143–144**, 347–356.
- Cordier, P., Ungár, T., Zsoldos, L. & Tichy, G. (2003). *Nature (London)*, **428**, 837–840.

- Duffy, T. S., Shen, G., Heinz, D. L., Shu, J., Ma, Y., Mao, H. K., Hemley, R. J. & Singh, A. K. (1999a). *Phys. Rev. B*, **60**, 15063–15073.
- Duffy, T. S., Shen, G., Shu, J., Mao, H. K., Hemley, R. J. & Singh, A. K. (1999b). *J. Appl. Phys.* **86**, 6729–6736.
- Durham, W. B., Mei, S., Kohlstedt, D. L., Wang, L. & Dixon, N. A. (2009). *Phys. Earth Planet. Inter.* **172**, 67–73.
- Durham, W. B. & Rubie, D. C. (1998). *Properties of Earth and Planetary Materials at High Pressure and Temperature, Geophysical Monograph 101*, edited by M. Manghnani and Y. Yagi, pp. 63–70. American Geophysical Union.
- Durham, W. B., Weidner, D. J., Karato, S.-I. & Wang, Y. (2002). *Plastic Deformation of Minerals and Rocks*, edited by S.-I. Karato and H.-R. Wenk, pp. 21–49. San Francisco: Mineralogical Society of America.
- Funamori, N., Yagi, T. & Uchida, T. (1994). *J. Appl. Phys.* **75**, 4327–4331.
- Gotou, H., Yagi, T., Frost, D. J. & Rubie, D. C. (2006). *Rev. Sci. Instrum.* **77**, 035113.
- He, D., Shieh, S. & Duffy, T. S. (2004). *Phys. Rev. B*, **70**, 184121.
- Hemley, R. J., Mao, H. K., Shen, G., Badro, J., Gillet, P., Hanfland, M. & Häusermann, D. (1997). *Science*, **276**, 1242–1245.
- Hilairt, N., Reynard, B., Wang, Y., Daniel, I., Merkel, S., Nishiyama, N. & Petitgirard, S. (2007). *Science*, **318**, 1910–1913.
- Jung, H. & Green, H. W. (2009). *Nat. Geosci.* **2**, 73–77.
- Karato, S. & Rubie, D. C. (1997). *J. Geophys. Res.* **102**, 20111–20122.
- Kavner, A. (2003). *Earth Planet. Sci. Lett.* **214**, 645–654.
- Kavner, A. (2007). *J. Geophys. Res.* **112**, B12207.
- Kavner, A. (2008). *Phys. Rev. B*, **77**, 224102.
- Kavner, A. & Duffy, T. S. (2001). *Geophys. Res. Lett.* **28**, 2691–2694.
- Kavner, A. & Duffy, T. S. (2003). *Phys. Rev. B*, **68**, 144101.
- Kawazoe, T., Karato, S. I. & Otsuka, K. (2009). *Phys. Earth Planet. Inter.* **174**, 128–137.
- Kiefer, B., Shieh, S. R., Duffy, T. S. & Sekine, T. (2005). *Phys. Rev. B*, **72**, 014102.
- Kinsland, G. L. & Bassett, W. A. (1976). *Rev. Sci. Instrum.* **47**, 130–132.
- Kocks, U. F., Tomé, C. N. & Wenk, H.-R. (1998). *Texture and Anisotropy*, p. 675. Cambridge University Press.
- Kunz, M., Caldwell, W. A., Miyagi, L. & Wenk, H. R. (2007). *Rev. Sci. Instrum.* **78**, 063907.
- Li, L., Long, H., Raterron, P. & Weidner, D. (2006a). *Am. Mineral.* **91**, 517–525.
- Li, L., Weidner, D. J., Chen, J., Vaughan, M. T. & Davis, M. (2004a). *J. Appl. Phys.* **95**, 8357–8365.
- Li, L. & Weidner, D. J. (2007). *Rev. Sci. Instrum.* **78**, 053902.
- Li, L. & Weidner, D. J. (2008). *Nature (London)*, **454**, 984–986.
- Li, L., Weidner, D., Raterron, P., Chen, J. & Vaughan, M. (2004b). *Phys. Earth Planet. Inter.* **143–144**, 357–367.
- Li, L., Weidner, D. J., Raterron, P., Chen, J., Vaughan, M. T., Shenghua, M. & Durham, W. B. (2006b). *Eur. J. Mineral.* **18**, 7–19.
- Liermann, H.-P., Merkel, S., Miyagi, L., Wenk, H. R., Shen, G., Cynn, H. & Evans, W. J. (2009). *Rev. Sci. Instrum.* In the press.
- Lutterotti, L., Matthies, S. & Wenk, H. R. (1999). *IUCr CPD Newslett.* **21**, 14–15.
- Mao, H. K., Badro, J., Shu, J., Hemley, R. J. & Singh, A. K. (2006). *J. Phys. Condens. Matter*, **18**, S963–S968.
- Mao, H. K., Shu, J., Shen, G., Hemley, R. J., Li, B. & Singh, A. K. (1998). *Nature (London)*, **396**, 741–743.
- Matthies, S., Priesmeyer, H. G. & Daymond, M. R. (2001). *J. Appl. Cryst.* **34**, 585–601.
- Matthies, S. & Vinel, G. W. (1982). *Phys. Status Solidi B*, **112**, K111–K114.
- Mei, S., Kohlstedt, D. L., Durham, W. B. & Wang, L. (2008). *Phys. Earth Planet. Inter.* **170**, 170–175.
- Merkel, S., Hemley, R. J., Mao, H. K. & Teter, D. M. (2000). *Science and Technology of High Pressure Research*, pp. 68–73. Hyderabad: Universities Press.
- Merkel, S., Kubo, A., Miyagi, L., Speziale, S., Duffy, T. S., Mao, H. K. & Wenk, H. R. (2006a). *Science*, **311**, 644–646.
- Merkel, S., McNamara, A. K., Kubo, A., Speziale, S., Miyagi, L., Meng, Y., Duffy, T. S. & Wenk, H. R. (2007). *Science*, **316**, 1729–1732.
- Merkel, S., Miyajima, N., Antonangeli, D., Fiquet, G. & Yagi, T. (2006b). *J. Appl. Phys.* **100**, 023510.
- Merkel, S., Tomé, C. & Wenk, H.-R. (2009). *Phys. Rev. B*, **79**, 064110.
- Merkel, S., Wenk, H. R., Badro, J., Montagnac, G., Gillet, P., Mao, H. K. & Hemley, R. J. (2003). *Earth Planet. Sci. Lett.* **209**, 351–360.
- Merkel, S., Wenk, H. R., Gillet, P., Mao, H. K. & Hemley, R. J. (2004). *Phys. Earth Planet. Inter.* **145**, 239–251.
- Merkel, S., Wenk, H. R., Shu, J., Shen, G., Gillet, P., Mao, H. K. & Hemley, R. J. (2002). *J. Geophys. Res.* **107**, 2271.
- Merkel, S. & Yagi, T. (2005). *Rev. Sci. Instrum.* **76**, 046109.
- Miyagi, L., Kunz, M., Knight, J., Nasiatka, J., Voltolini, M. & Wenk, H.-R. (2008). *J. Appl. Phys.* **104**, 103510.
- Miyagi, L., Merkel, S., Yagi, T., Sata, N., Ohishi, Y. & Wenk, H. R. (2009). *Phys. Earth Planet. Inter.* **174**, 159–164.
- Miyagi, L., Nishiyama, N., Wang, Y., Kubo, A., West, D. V., Cava, R. J., Duffy, T. S. & Wenk, H. R. (2008). *Earth Planet. Sci. Lett.* **268**, 515–525.
- Nishihara, Y., Tinker, D., Kawazoe, T., Xu, Y., Jing, Z., Matsukage, K. N. & Karato, S. (2008). *Phys. Earth Planet. Inter.* **170**, 156–169.
- Nishiyama, N., Wang, Y., Irifune, T., Sanehira, T., Rivers, M. L., Sutton, S. R. & Cookson, D. (2009). *J. Synchrotron Rad.* **16**, 742–747.
- Nishiyama, N., Wang, Y., Rivers, M. L., Sutton, S. R. & Cookson, D. (2007). *Geophys. Res. Lett.* **34**, L23304.
- Nishiyama, N., Wang, Y., Uchida, T., Irifune, T., Rivers, M. L. & Sutton, S. R. (2005). *Geophys. Res. Lett.* **32**, L04307.
- Raterron, P., Amiguet, E., Chen, J., Li, L. & Cordier, P. (2009). *Phys. Earth Planet. Inter.* **172**, 74–83.
- Raterron, P., Chen, J., Li, L., Weidner, D. & Cordier, P. (2007). *Am. Mineral.* **92**, 1436–1445.
- Raterron, P., Wu, Y., Weidner, D. J. & Chen, J. (2004). *Phys. Earth Planet. Inter.* **145**, 149–159.
- Shieh, S., Duffy, T. S. & Li, B. (2002). *Phys. Rev. Lett.* **89**, 255507.
- Shieh, S. R., Duffy, T. S. & Shen, G. (2004). *Phys. Earth Planet. Inter.* **143–144**, 93–105.
- Singh, A. K., Balasingh, C., Mao, H. K., Hemley, R. J. & Shu, J. (1998). *J. Appl. Phys.* **83**, 7567–7575.
- Speziale, S., Lonardelli, I., Miyagi, L., Pehl, J., Tommaseo, C. E. & Wenk, H. R. (2006a). *J. Phys. Condens. Matter*, **18**, S1007–S1020.
- Speziale, S., Shieh, S. R. & Duffy, T. S. (2006b). *J. Geophys. Res.* **111**, B02203.
- Tommaseo, C. E., Devine, J., Merkel, S., Speziale, S. & Wenk, H. R. (2006). *Phys. Chem. Miner.* **33**, 84–97.
- Uchida, T., Funamori, N., Ohtani, T. & Yagi, T. (1996). *High Pressure Science and Technology*, edited by W. A. Trzcianowski, pp. 183–185. Singapore: World Scientific.
- Uchida, T., Wang, Y., Rivers, M. L. & Sutton, S. R. (2004). *Earth Planet. Sci. Lett.* **226**, 117–126.
- Vaughan, M., Chen, J., Li, L., Weidner, D. & Li, B. (2000). *International Conference on High Pressure Science and Technology – AIRAPT-17*, edited by M. H. Manghnani, W. J. Nellis and M. F. Nicol, pp. 1097–1098. Hyderabad: Universities Press.
- Walte, N. P., Heidelberg, F., Miyajima, N., Frost, D. J., Rubie, D. C. & Dobson, D. P. (2009). *Geophys. Res. Lett.* **36**, L04302.
- Wang, Y., Durham, W., Getting, I. C. & Weidner, D. (2003). *Rev. Sci. Instrum.* **74**, 3002–3011.
- Wang, L., Weidner, D. J., Vaughan, M. T., Chen, J., Li, B. & Liebermann, R. C. (2007). *EOS Trans. AGU*, **88**(52), Fall Meeting Supplement, Abstract MR53A-01.
- Weidner, D. J., Li, L., Davis, M. & Chen, J. (2004). *Geophys. Res. Lett.* **31**, L06621.
- Weidner, D. J., Li, L., Durham, W. & Chen, J. (2005). *Advances in High-Pressure Technology for Geophysical Applications*, edited by

- J. Chen, Y. Wang, T. S. Duffy, G. Shen and L. F. Dobrzhinetskaya, pp. 123–136. Amsterdam: Elsevier.
- Weinberger, M. B., Tolbert, S. H. & Kavner, A. (2008). *Phys. Rev. Lett.* **100**, 045506.
- Wenk, H. R., Ischia, G., Nishiyama, N., Wang, Y. & Uchida, T. (2005). *Phys. Earth Planet. Inter.* **152**, 191–199.
- Wenk, H. R., Lonardelli, I., Merkel, S., Miyagi, L., Pehl, J., Speziale, S. & Tommaseo, C. E. (2006). *J. Phys. Condens. Matter*, **18**, S933–S947.
- Wenk, H. R., Lonardelli, I., Pehl, J., Devine, J., Prakapenka, V., Shen, G. & Mao, H. K. (2004). *Earth Planet. Sci. Lett.* **226**, 507–519.
- Wenk, H.-R., Matthies, S., Donovan, J. & Chateigner, D. (1998). *J. Appl. Cryst.* **31**, 262–269.
- Wenk, H. R., Matthies, S., Hemley, R. J., Mao, H. K. & Shu, J. (2000). *Nature (London)*, **405**, 1044–1047.
- Xu, Y., Nishihara, Y. & Karato, S. (2005). *Advances in High-Pressure Technology for Geophysical Applications*, edited by J. Chen, Y. Wang, T. S. Duffy, G. Shen and L. F. Dobrzhinetskaya, pp. 167–182. Amsterdam: Elsevier.
- Yamazaki, D. & Karato, S. (2001). *Rev. Sci. Instrum.* **72**, 4207–4211.
- Zhang, S. & Karato, S. (1995). *Nature (London)*, **375**, 774–777.